

Identification of a Helium Donor Star in NGC 247 ULX-1

CHANGXING ZHOU,¹ HUA FENG,^{2,1} AND FUYAN BIAN³

¹*Department of Engineering Physics, Tsinghua University, Beijing 100084, China*

²*Department of Astronomy, Tsinghua University, Beijing 100084, China; hfeng@tsinghua.edu.cn*

³*European Southern Observatory, Alonso de Córdova 3107, Casilla 19001, Vitacura, Santiago 19, Chile; fuyan.bian@eso.org*

ABSTRACT

With Very Large Telescope (VLT) Multi Unit Spectroscopic Explorer (MUSE) observations, we detected highly variable helium emission lines from the optical counterpart of the supersoft ultraluminous X-ray source (ULX) NGC 247 ULX-1. No Balmer lines can be seen in the source spectrum. This is the first evidence for the presence of a helium donor star in ULXs, consistent with a prediction that helium donor stars may be popular in ULXs. The helium lines with a FWHM of about 200 km s⁻¹ are likely produced on the outer accretion disk. Their strong variation implies that the central X-ray source can be significantly obscured to the outer disk. Also, a ring or a double-ring structure is revealed in the MUSE image. It is unknown whether or not it is related to the progenitor of the ULX binary.

1. INTRODUCTION

Ultraluminous X-ray sources (ULXs) are non-nuclear accreting compact objects with an apparent luminosity above the Eddington limit of stellar mass black holes (Fabbiano 1989; Makishima et al. 2000). Identifications of high velocity (~ 0.1 – $0.4 c$) outflows (Pinto et al. 2016, 2017, 2021; Walton et al. 2016; Kosec et al. 2018), energetic shock-ionized bubble nebulae (Pakull & Mirioni 2002, 2003; Ramsey et al. 2006; Abolmasov & Moiseev 2008; Russell et al. 2011; Belfiore et al. 2020; Soria et al. 2021; Zhou et al. 2022), and neutron star accretors (Bachetti et al. 2014; Fürst et al. 2016; Israel et al. 2017a,b; Carpano et al. 2018; Sathyaprakash et al. 2019; Rodríguez Castillo et al. 2020), suggest that the majority of them are powered by supercritical accretion.

Observations of the optical counterpart of ULXs may shed light on the history of binary evolution (Madhusudhan et al. 2008; Patruno & Zampieri 2008), and place constraints on the accretion geometry (Vinokurov et al. 2013; Ambrosi & Zampieri 2018; Yao & Feng 2019) and compact object mass (Liu et al. 2013; Motch et al. 2014). However, due to their extragalactic distances, spectroscopic observations of their optical counterparts are challenging and only available for a limited number of sources (Abolmasov et al. 2007; Roberts et al. 2011; Tao et al. 2012; Cseh et al. 2013; Fabrika et al. 2015; Heida et al. 2015, 2016; Vinokurov et al. 2018; Heida et al. 2019; López et al. 2020).

Most ULXs are argued to be viewed close to face-on, but there is a class of supersoft ULXs (e.g., Read & Pietsch 2001; Fabbiano et al. 2003; Liu et al. 2015; Soria & Kong 2016), whose X-ray spectrum is dominated by emission below 1 keV, speculated to be viewed close to edge-on (for a review see Kaaret et al. 2017). Thus, these sources could be

ideal targets for dynamical measurements using optical spectroscopy. NGC 247 ULX-1 is a typical one in this class (Jin et al. 2011). Mildly relativistic wind with a velocity of $0.17 c$ is detected in it (Pinto et al. 2021). The source displays frequent dips in the X-ray lightcurve, with transitions between a supersoft regime with little emission above 1 keV and a soft regime with enhanced hard X-ray emission (Feng et al. 2016; Alston et al. 2021; D’Aì et al. 2021). The optical counterpart of NGC 247 ULX-1 was identified by aligning the Chandra and Hubble Space Telescope (HST) images (Tao et al. 2012), has a spectral energy density peaked in the UV band (Feng et al. 2016), which can be reasonably explained as due to self-irradiation from an optically thick wind as a natural consequence of supercritical accretion (Yao & Feng 2019). All the above observational features can be interpreted as a result of supercritical accretion viewed at a high inclination angle. In this paper, we present Very Large Telescope (VLT) observations of NGC 247 ULX-1 with the Multi Unit Spectroscopic Explorer (MUSE) instrument (Bacon et al. 2010).

2. OBSERVATION AND DATA ANALYSIS

NGC 247 ULX-1 was observed with VLT MUSE on 2022 May 27 and May 30, respectively, at the La Silla Paranal Observatory under the program 109.238W.002. Each observation contains 4×560 s on-source exposures and 2×120 s sky exposures. A 90 degree rotation plus small offset dithering patterns was applied between the on-source exposures. The seeing was $0''.5$ – $0''.7$ during the observations. The sky transparency conditions were clear on the night of May 27, and partially cloudy on the night of May 30. The instru-

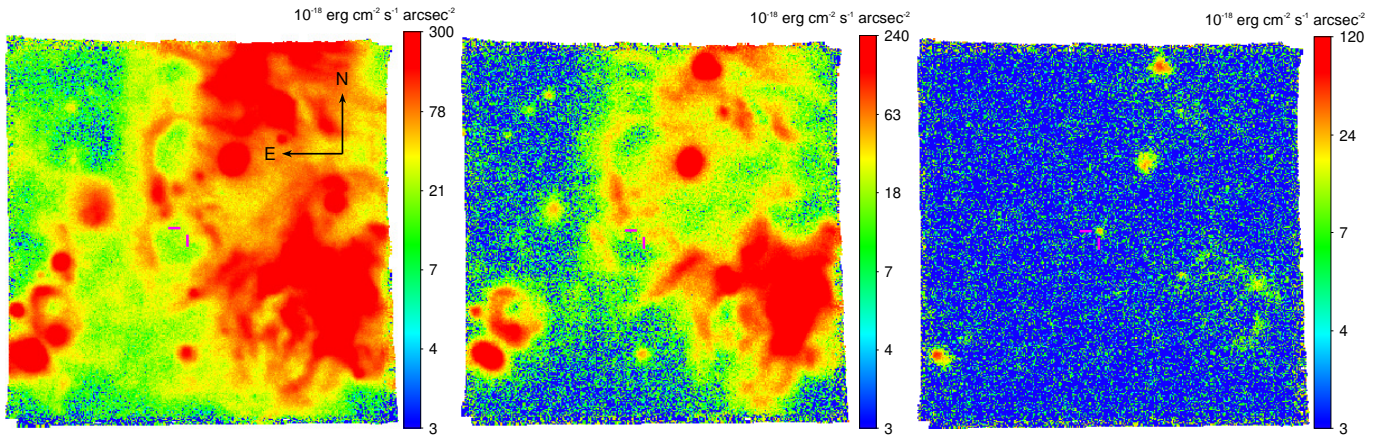


Figure 1. MUSE flux images around NGC 247 ULX-1 for $H\alpha$ (left), $[O\text{ III}]\lambda 5007$ (middle), and $\text{He I}\lambda 6678$ (right), respectively, from combined observations. For $H\alpha$ and $[O\text{ III}]\lambda 5007$, the flux is extracted from a 10\AA window around the line centroid; for $\text{He I}\lambda 6678$, the extraction window is 11.25\AA . The continuum is estimated from nearby wavelengths free of line features and subtracted. The bars marks the position of the optical counterpart to NGC 247 ULX-1 (Tao et al. 2012). The arrows points north and east, respectively, with a length of $10''$.

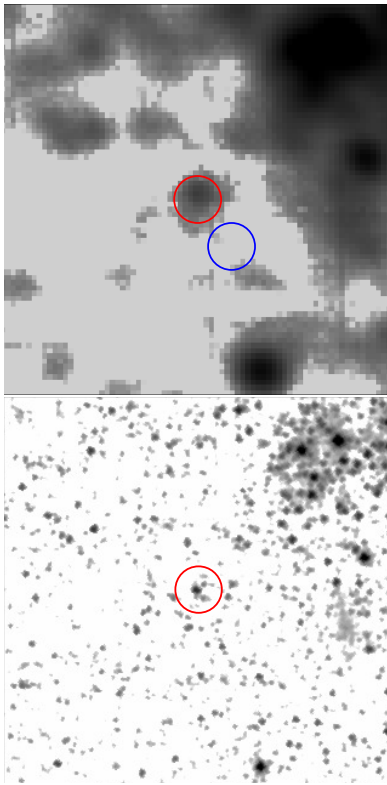


Figure 2. **Top:** MUSE image around NGC 247 ULX-1 in the HST ACS WFC F606W filter from combined observations. The red aperture encircles the optical counterpart of the ULX and the blue circle marks the background region, both with a radius of $0''.9$. **Bottom:** HST ACS WFC F606W image (dataset jblm01030) adopted from Tao et al. (2012), smoothed with a Gaussian kernel ($\sigma = 1.5$ pixel). The size of the images is $15'' \times 15''$.

ment mode used was WFM-NOAO-E, covering a wavelength range of $4600\text{--}9350\text{\AA}$.

The data were reduced by the EsoRex pipeline. For each independent exposure, we used the *muse_scibasic* recipe to

Table 1. Emission line flux, velocity, and velocity dispersion for the optical counterpart of the ULX.

Line	flux			v	FWHM
	$(10^{-18}\text{ erg cm}^{-2}\text{ s}^{-1})$			(km s^{-1})	(km s^{-1})
	May 27	May 30	Total	Total	Total
$\text{He II}\lambda 4686$	< 3	33 ± 9	14 ± 5	106 ± 24	120 ± 106
$\text{He I}\lambda 5876$	39 ± 5	50 ± 5	42 ± 4	79 ± 10	281 ± 29
$\text{He I}\lambda 6678$	23 ± 3	32 ± 3	26 ± 2	57 ± 6	183 ± 16
$\text{He I}\lambda 7065$	27 ± 6	45 ± 6	34 ± 4	57 ± 9	246 ± 24

NOTE— v is the relative velocity with respect to the host galaxy. FWHM has been corrected for instrument line broadening. Nondetections are quoted as 90% upper limits. Line fluxes are obtained from the two individual spectra and the total spectrum, respectively, while v and FWHM are obtained from the total spectrum.

correct the bias frames, lamp flats, arc lamps, twilight flats, geometry, and illumination exposures. With standard stars taken on the same night, *muse_scipost* was employed to correct the telluric and flux. We used *muse_exp_align* to align each exposure, and *muse_exp_combine* to generate the final data cube. The field of view of the final data cube is $1' \times 1'$, with the spaxel scale $0''.2 \times 0''.2$.

Figure 1 shows the MUSE emission line flux images for $H\alpha$, $[O\text{ III}]\lambda 5007$, and $\text{He I}\lambda 6678$. The flux is summed around the line centroid and the continuum is estimated from nearby wavelengths and subtracted. The position of the optical counterpart to NGC 247 ULX-1 is adopted from Tao et al. (2012) and marked in the plot. As one can see, there is a point-like source in the ULX region in the $\text{He I}\lambda 6678$ image but not in the $H\alpha$ and $[O\text{ III}]\lambda 5007$ images.

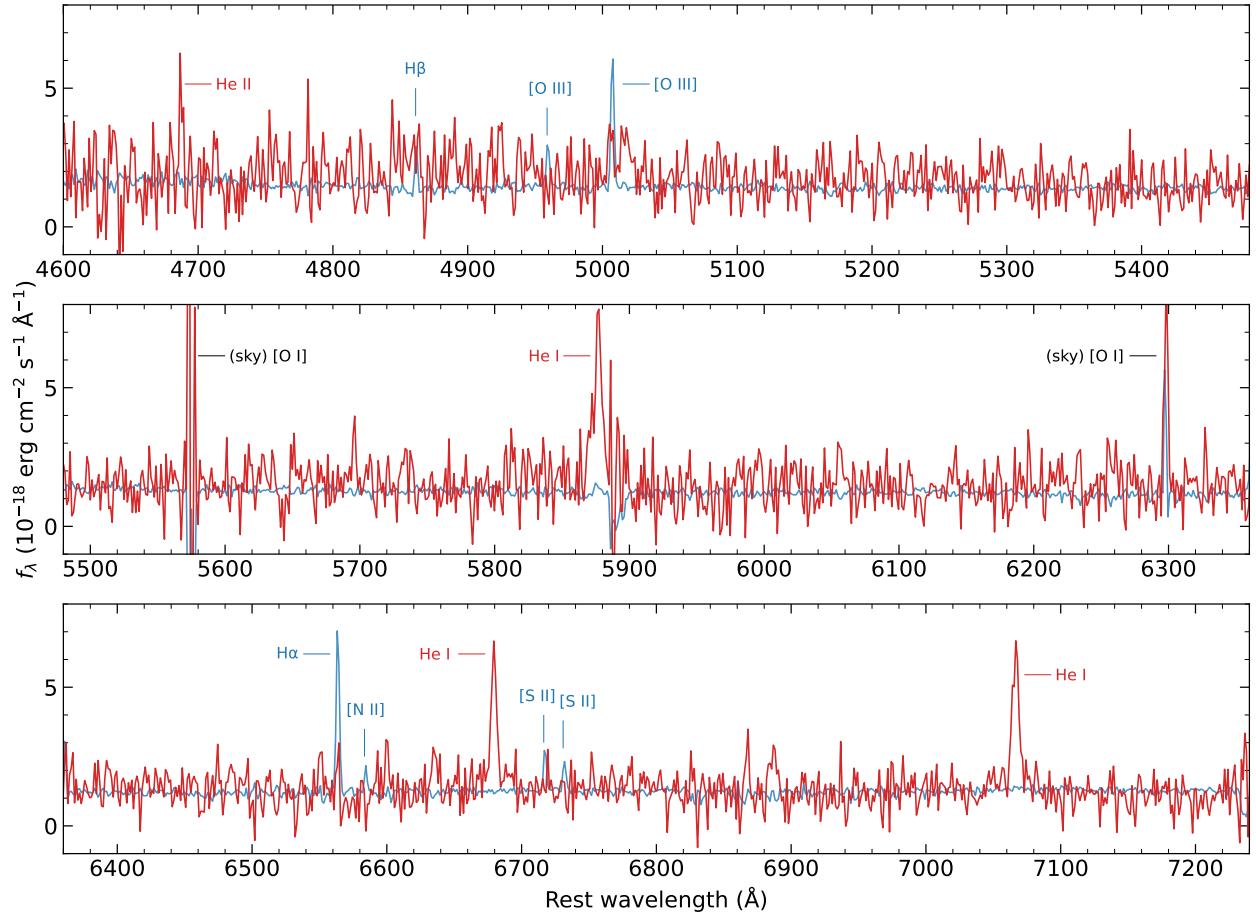


Figure 3. MUSE spectrum of the ULX optical counterpart in the wavelength range of 4600–7240 Å from combined observations. The red curve is the background subtracted ULX spectrum, and the blue curve is the background spectrum divided by a factor of 400, extracted from the blue circle region in Figure 2. Significant emission lines and sky lines are indicated.

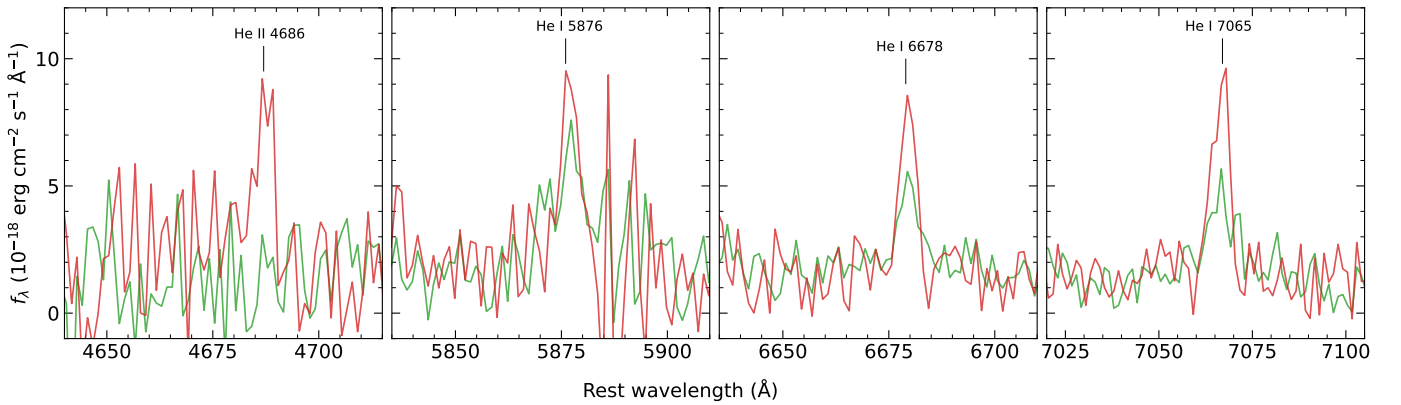


Figure 4. Spectra around helium emission lines of the ULX optical counterpart obtained from the two individual observations on May 27 (green) and May 30 (red).

To compare with the HST ACS WFC F606W image, we plot the MUSE image extracted in the same filter, shown in Figure 2. Bright and isolated point-like sources are used to align the two images. In the MUSE image, there is an object around the ULX position, with a radial profile well consistent with that of nearby point-like sources. The radius that encircles 90% of the source flux is $0''.9$, adopted as the source aperture. In the HST image, the optical counterpart of the ULX is the dominant source within the aperture. Thus, the MUSE object in the aperture is mainly attributed to emission from the ULX optical counterpart.

The absence of the ULX optical counterpart in the $H\alpha$ image (Figure 1) suggests that the $H\alpha$ emission from the source is negligible compared with the diffuse component in the local environment. Therefore, we should choose a background region where the diffuse $H\alpha$ intensity is similar as in the source aperture. The background region is chosen with the aid of the $H\alpha$ contour map and shown as a blue circle in Figure 2. The background subtracted spectrum for the ULX optical counterpart is displayed in Figure 3.

Several emission lines can be identified from the spectrum. Each emission line is fitted locally with a Gaussian after subtraction of the continuum. The continuum is determined with a linear function from nearby wavelengths free of the emission component. The line flux, velocity relative to the host galaxy ($z = 0.000520$ or $v = 156 \text{ km s}^{-1}$; Koribalski et al. 2004), and the FWHM velocity dispersion corrected for instrument line broadening are listed in Table 1. We note that there are a few other helium lines that can be barely seen; we do not report them due to low signal-to-noise ratios. For $H\alpha$, we estimate a 90% upper limit of $6 \times 10^{-19} \text{ erg cm}^{-2} \text{ s}^{-1}$.

The optical spectrum shows no detectable Balmer lines, consistent with what one can see from the $H\alpha$ image. The most prominent lines are the He I lines. He II $\lambda 4686$ can be detected at a significance close to 3σ . The [O III] $\lambda 5007$ line may arise from the local diffuse component due to incomplete background subtraction, as one can see from Figure 1 that the [O III] $\lambda 5007$ emission in the background region is slightly lower than in the aperture. We checked the background spectrum (also shown in Figure 3) and find no helium emission lines.

The MUSE data contain two individual observations on May 27 and 30, respectively, with a separation of nearly 3 days. To investigate the line variability, we compare the emission line flux obtained from the two individual observations, also listed in Table 1. The spectra for several helium lines that show strong variations are displayed in Figure 4. Emission line fluxes from nearby star forming regions are used for relative flux calibration, applied on the spectrum on May 30, with an accuracy estimated to be better than 1%.

Another interesting feature that can be seen in the $H\alpha$ and [O III] images (Figure 1) around the ULX position is a ring

Table 2. The emission line flux and velocity for the double-ring structure.

line	flux ($10^{-16} \text{ erg cm}^{-2} \text{ s}^{-1}$)	v (km s^{-1})
$H\beta$	15.49 ± 0.28	41.4 ± 1.9
[O III] $\lambda 4959$	11.01 ± 0.14	46.5 ± 1.2
[O III] $\lambda 5007$	32.81 ± 0.41	46.5 ± 1.2
$H\alpha$	56.02 ± 0.41	44.6 ± 0.5
[N II] $\lambda 6583$	5.41 ± 0.14	42.3 ± 1.9
[S II] $\lambda 6716$	8.74 ± 0.12	45.0 ± 0.7
[S II] $\lambda 6731$	5.49 ± 0.12	45.0 ± 0.7

NOTE— v is the relative velocity with respect to the host galaxy. The intrinsic line width is fixed at zero.

structure, which is possibly part of an “8” shaped double-ring structure. The spectrum extracted from some parts of the double-ring structure (to avoid the western star forming region) is displayed in Figure 5. The spectra from different extraction regions look similar, and we thus just display the total spectrum. Each emission line is fitted with a Gaussian, with the line properties listed in Table 2. The intrinsic line width cannot be resolved and is fixed at zero in the fits. For $H\alpha$, the 90% upper limit of the line FWHM is constrained to be 35 km s^{-1} , suggesting that the double-ring structure is due to photoionization instead of shock ionization. The same conclusion can be obtained with the emission line diagnostic diagram (Baldwin et al. 1981).

3. DISCUSSION

In this work, we detected highly variable helium lines from the optical counterpart of NGC 247 ULX-1 with VLT MUSE observations. The dramatic variation indicates that the emission lines arise from the accretion system. The absence of Balmer lines and richness of helium lines suggests that the mass donor in the X-ray binary is a hydrogen-deficient star.

Shao et al. (2019) performed a population synthesis study to investigate the neutron star population in ULXs. Combined with detailed calculations of stellar and binary evolutions, they found that in a Milky Way-like galaxy a significant fraction of ULXs are neutron star X-ray binaries containing a helium star companion. The helium star was formed in the common envelope phase during which the hydrogen envelope of its progenitor was stripped (also see Quast et al. 2019; Abdusalam et al. 2020; Götberg et al. 2020; Wang et al. 2021). Our finding is consistent with their prediction and is the first smoking gun evidence for the presence of a helium donor star in ULXs. Interestingly, Shao et al. (2019) showed

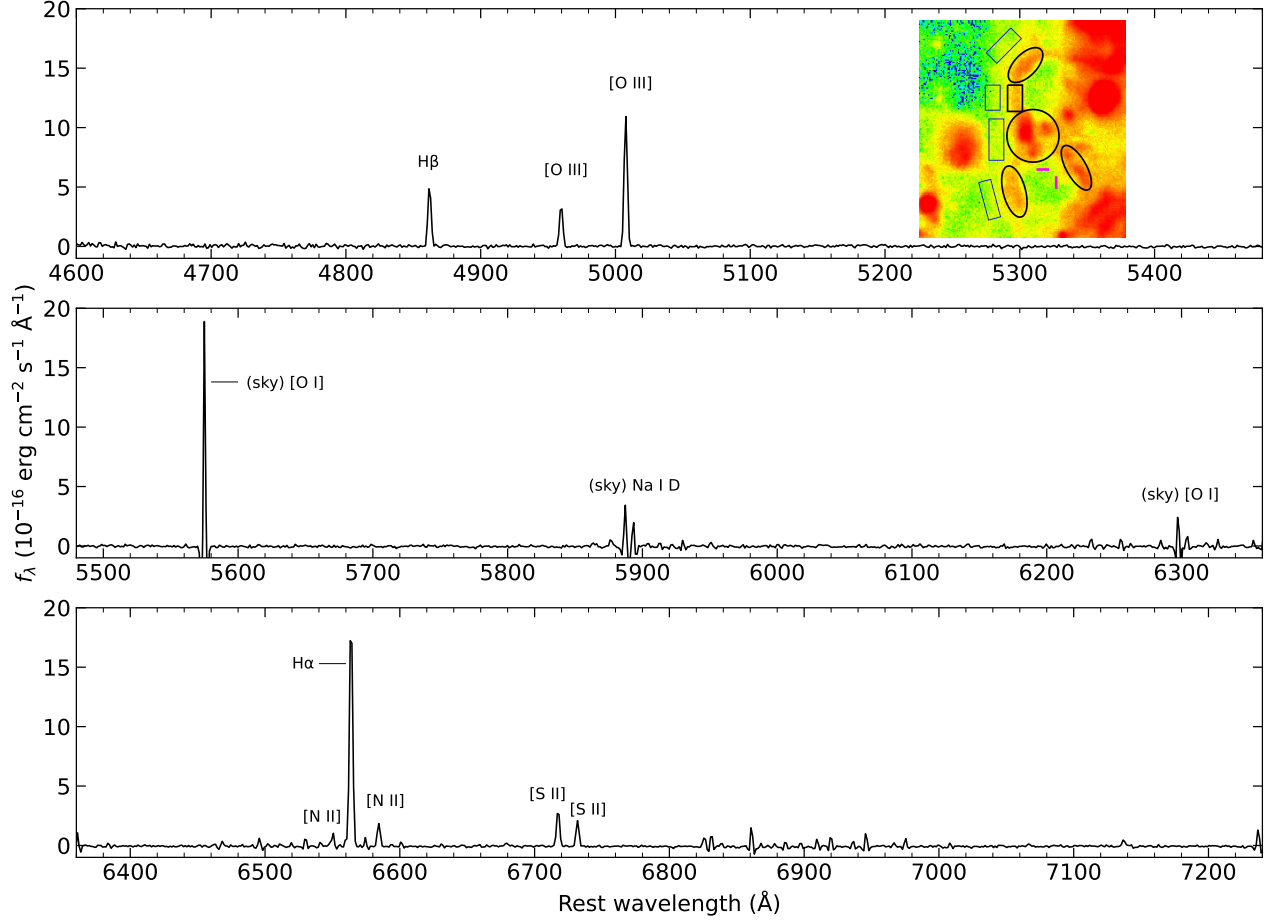


Figure 5. Background subtracted spectrum from some parts of the double-ring structure from the combined observation. The inset H α image shows the extraction regions for the source (thick black) and background (thin blue), and the bars indicate the ULX position. Significant emissions lines are marked.

that such systems are likely close binaries with an orbital period distribution peaked at 0.1 day, and the helium star mass ranges from $0.6\text{--}2 M_{\odot}$.

For NGC 247 ULX-1, no coherent pulsation was detected with a long XMM observation (D’Aì et al. 2021). However, this cannot rule out that it contains a neutron star, because the observed X-ray emission may have been largely reprocessed in the wind leading to a low pulsed fraction. Plus, a sufficiently high spin-up rate may be needed for a neutron star ULX to appear as a pulsar (King et al. 2017). Like other soft ULXs, NGC 247 ULX-1 exhibits dips in its lightcurve (Feng et al. 2016). The dips seem to occur randomly in time, and there is no evidence that they are caused by binary motion (D’Aì et al. 2021; Alston et al. 2021).

The FWHM of the He I emission lines is about $180\text{--}280 \text{ km s}^{-1}$. If we assume a neutron star accretor with a mass of $1.4 M_{\odot}$, the FWHM/2 corresponds to a Keplerian velocity at a radius of roughly $(0.5 - 2.0) \times 10^{12} \text{ cm}$ if the

inclination angle is in the range of $45\text{--}80 \text{ deg}$ (the inclination is supposed to be large but there is no eclipse). Adopting a donor star mass of $0.6\text{--}2 M_{\odot}$ (Shao et al. 2019), this requires a binary orbital period of at least $2.4\text{--}21 \text{ day}$ (Eggleton 1983) for the Roche-lobe radius around the compact object to be larger than the above radius. This is larger than the most likely orbital period predicted by Shao et al. (2019), but is consistent with the range of distribution that they predicted. Thus, an outer disk origin for the He I line is possible in this scenario. Emission lines on the outer accretion disk are supposed to show a double-peak profile, which, however, cannot be detected given the spectral resolution and signal-to-noise ratio of the data. The strong variation of the helium lines implies that the central X-ray source can be largely obscured to the outer accretion disk. Compared with the emission line measured in other ULXs (e.g., Fabrika et al. 2015), the line width in NGC 247 ULX-1 is much smaller ($200 \text{ vs. } 400\text{--}1800 \text{ km s}^{-1}$), not in support of the scenario that the

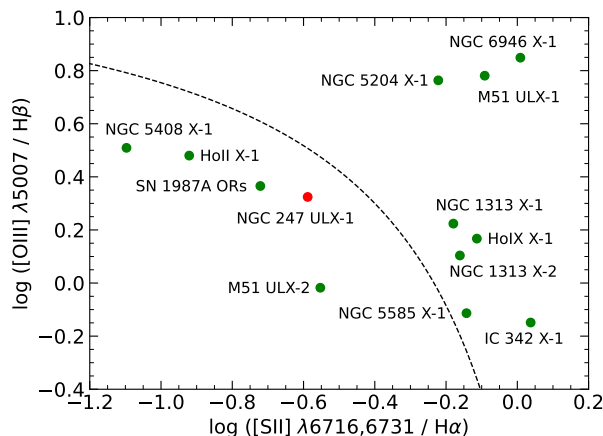


Figure 6. The emission line diagnostic diagram (Baldwin et al. 1981) for the double-ring structure around NGC 247 ULX-1, ULX bubbles including Holmberg II X-1 (Lehmann et al. 2005), Holmberg IX X-1 (Abolmasov et al. 2007), IC 342 X-1 (Roberts et al. 2003), M51 ULX (Urquhart et al. 2018), NGC 1313 X-1 (Gúrpide et al. 2022) and X-2 (Zhou et al. 2022), NGC 5204 X-1 (Abolmasov et al. 2007), NGC 5408 X-1 (Kaaret & Corbel 2009; Cseh et al. 2012), NGC 5585 X-1 (Soria et al. 2021), NGC 6946 X-1 (Abolmasov et al. 2007), and the SN 1987A outer rings (Tziamtzis et al. 2011). The dashed curve adopted from Kewley et al. (2001) separates photoionization and shock ionization.

lines are originating from the base of the accelerating wind as argued for other sources. As per the prediction of Shao et al. (2019) and above estimates, it would be interesting to search for signatures of binary modulation at a period of several days, although the predicted binary period could be as long as 100 days with a low probability.

There is no evidence that the nearby ring or double-ring structure is related to the ULX. One possible conjecture would be that the ring or even the double-ring structure was

produced by the progenitor of the compact object in the ULX binary, e.g., similar to one of the scenarios for the formation of the outer rings around the supernova SN 1987A due to magnetically confined anisotropic stellar ejections (Tanaka & Washimi 2002), although their spatial sizes are distinct. The ULX binary was kicked off and moved away from the center of the structure to its current position after the supernova explosion. In that case, if we assume that the binary is originally at the center of the southern ring or the conjunction region of the two rings (with an angular distance of $3''$ – $5''$), a kick-off velocity of at least 5 – 8 km s $^{-1}$ can be inferred given a typical age of 10 Myr (Tao et al. 2012) and a distance of 3.4 Mpc to the galaxy (Gieren et al. 2009). This is consistent with the velocity difference between the ULX counterpart and ring structure (see Tables 1 & 2).

The small line width and also the line flux ratios suggest that the double-ring structure is a result of photoionization instead of shock ionization. To compare it with other ULX bubbles (e.g., Pakull & Mirioni 2002) as well as the SN 1987A outer rings, we plot their line ratios on the Baldwin et al. (1981) diagnostic diagram, see Figure 6. It can be seen that the double-ring structure around NGC 247 ULX-1 is similar to the nebula around Holmberg II X-1 (Lehmann et al. 2005) and the SN 1987A outer rings (Tziamtzis et al. 2011), both of which are due to photoionization.

We thank the anonymous referee for useful comments. HF acknowledges funding support from the National Key R&D Project under grant 2018YFA0404502, the National Natural Science Foundation of China under grants Nos. 12025301, 12103027, & 11821303, and the Tsinghua University Initiative Scientific Research Program. Some of the data presented in this paper were obtained from the Mikulski Archive for Space Telescopes (MAST) at the Space Telescope Science Institute. The specific observations analyzed can be accessed via DOI: 10.17909/trtf-5s84.

REFERENCES

- Abdusalam, K., Ablimit, I., Hashim, P., et al. 2020, *ApJ*, 902, 125, doi: 10.3847/1538-4357/abb5a8
- Abolmasov, P., Fabrika, S., Sholukhova, O., & Afanasiev, V. 2007, *Astrophysical Bulletin*, 62, 36, doi: 10.1134/S199034130701004X
- Abolmasov, P., & Moiseev, A. V. 2008, *RMxAA*, 44, 301, doi: 10.48550/arXiv.0806.4527
- Alston, W. N., Pinto, C., Barret, D., et al. 2021, *MNRAS*, 505, 3722, doi: 10.1093/mnras/stab1473
- Ambrosi, E., & Zampieri, L. 2018, *MNRAS*, 480, 4918, doi: 10.1093/mnras/sty2213
- Bachetti, M., Harrison, F. A., Walton, D. J., et al. 2014, *Nature*, 514, 202, doi: 10.1038/nature13791
- Bacon, R., Accardo, M., Adjali, L., et al. 2010, in *Society of Photo-Optical Instrumentation Engineers (SPIE) Conference Series*, Vol. 7735, *Ground-based and Airborne Instrumentation for Astronomy III*, ed. I. S. McLean, S. K. Ramsay, & H. Takami, 773508, doi: 10.1117/12.856027
- Baldwin, J. A., Phillips, M. M., & Terlevich, R. 1981, *PASP*, 93, 5, doi: 10.1086/130766
- Belfiore, A., Esposito, P., Pintore, F., et al. 2020, *Nature Astronomy*, 4, 147, doi: 10.1038/s41550-019-0903-z

- Carpano, S., Haberl, F., Maitra, C., & Vasilopoulos, G. 2018, *MNRAS*, 476, L45, doi: [10.1093/mnras/sly030](https://doi.org/10.1093/mnras/sly030)
- Cseh, D., Grisé, F., Kaaret, P., et al. 2013, *MNRAS*, 435, 2896, doi: [10.1093/mnras/stt1484](https://doi.org/10.1093/mnras/stt1484)
- Cseh, D., Corbel, S., Kaaret, P., et al. 2012, *ApJ*, 749, 17, doi: [10.1088/0004-637X/749/1/17](https://doi.org/10.1088/0004-637X/749/1/17)
- D’Ài, A., Pinto, C., Del Santo, M., et al. 2021, *MNRAS*, 507, 5567, doi: [10.1093/mnras/stab2427](https://doi.org/10.1093/mnras/stab2427)
- Eggleton, P. P. 1983, *ApJ*, 268, 368, doi: [10.1086/160960](https://doi.org/10.1086/160960)
- Fabbiano, G. 1989, *ARA&A*, 27, 87, doi: [10.1146/annurev.aa.27.090189.000511](https://doi.org/10.1146/annurev.aa.27.090189.000511)
- Fabbiano, G., King, A. R., Zezas, A., et al. 2003, *ApJ*, 591, 843, doi: [10.1086/375441](https://doi.org/10.1086/375441)
- Fabrika, S., Ueda, Y., Vinokurov, A., Sholukhova, O., & Shidatsu, M. 2015, *Nature Physics*, 11, 551, doi: [10.1038/nphys3348](https://doi.org/10.1038/nphys3348)
- Feng, H., Tao, L., Kaaret, P., & Grisé, F. 2016, *ApJ*, 831, 117, doi: [10.3847/0004-637X/831/2/117](https://doi.org/10.3847/0004-637X/831/2/117)
- Fürst, F., Walton, D. J., Harrison, F. A., et al. 2016, *ApJL*, 831, L14, doi: [10.3847/2041-8205/831/2/L14](https://doi.org/10.3847/2041-8205/831/2/L14)
- Gieren, W., Pietrzyński, G., Soszyński, I., et al. 2009, *ApJ*, 700, 1141, doi: [10.1088/0004-637X/700/2/1141](https://doi.org/10.1088/0004-637X/700/2/1141)
- Götberg, Y., Korol, V., Lamberts, A., et al. 2020, *ApJ*, 904, 56, doi: [10.3847/1538-4357/abbda5](https://doi.org/10.3847/1538-4357/abbda5)
- Gúrpide, A., Parra, M., Godet, O., Contini, T., & Olive, J. F. 2022, *A&A*, 666, A100, doi: [10.1051/0004-6361/202142229](https://doi.org/10.1051/0004-6361/202142229)
- Heida, M., Jonker, P. G., Torres, M. A. P., et al. 2016, *MNRAS*, 459, 771, doi: [10.1093/mnras/stw695](https://doi.org/10.1093/mnras/stw695)
- Heida, M., Torres, M. A. P., Jonker, P. G., et al. 2015, *MNRAS*, 453, 3510, doi: [10.1093/mnras/stv1853](https://doi.org/10.1093/mnras/stv1853)
- Heida, M., Lau, R. M., Davies, B., et al. 2019, *ApJL*, 883, L34, doi: [10.3847/2041-8213/ab4139](https://doi.org/10.3847/2041-8213/ab4139)
- Israel, G. L., Belfiore, A., Stella, L., et al. 2017a, *Science*, 355, 817, doi: [10.1126/science.aai8635](https://doi.org/10.1126/science.aai8635)
- Israel, G. L., Papitto, A., Esposito, P., et al. 2017b, *MNRAS*, 466, L48, doi: [10.1093/mnras/slw218](https://doi.org/10.1093/mnras/slw218)
- Jin, J., Feng, H., Kaaret, P., & Zhang, S.-N. 2011, *ApJ*, 737, 87, doi: [10.1088/0004-637X/737/2/87](https://doi.org/10.1088/0004-637X/737/2/87)
- Kaaret, P., & Corbel, S. 2009, *ApJ*, 697, 950, doi: [10.1088/0004-637X/697/1/950](https://doi.org/10.1088/0004-637X/697/1/950)
- Kaaret, P., Feng, H., & Roberts, T. P. 2017, *ARA&A*, 55, 303, doi: [10.1146/annurev-astro-091916-055259](https://doi.org/10.1146/annurev-astro-091916-055259)
- Kewley, L. J., Dopita, M. A., Sutherland, R. S., Heisler, C. A., & Trevena, J. 2001, *ApJ*, 556, 121, doi: [10.1086/321545](https://doi.org/10.1086/321545)
- King, A., Lasota, J.-P., & Kluźniak, W. 2017, *MNRAS*, 468, L59, doi: [10.1093/mnras/slx020](https://doi.org/10.1093/mnras/slx020)
- Koribalski, B. S., Staveley-Smith, L., Kilborn, V. A., et al. 2004, *AJ*, 128, 16, doi: [10.1086/421744](https://doi.org/10.1086/421744)
- Kosec, P., Pinto, C., Walton, D. J., et al. 2018, *MNRAS*, 479, 3978, doi: [10.1093/mnras/sty1626](https://doi.org/10.1093/mnras/sty1626)
- Lehmann, I., Becker, T., Fabrika, S., et al. 2005, *A&A*, 431, 847, doi: [10.1051/0004-6361:20035827](https://doi.org/10.1051/0004-6361:20035827)
- Liu, J.-F., Bregman, J. N., Bai, Y., Justham, S., & Crowther, P. 2013, *Nature*, 503, 500, doi: [10.1038/nature12762](https://doi.org/10.1038/nature12762)
- Liu, J.-F., Bai, Y., Wang, S., et al. 2015, *Nature*, 528, 108, doi: [10.1038/nature15751](https://doi.org/10.1038/nature15751)
- López, K. M., Heida, M., Jonker, P. G., et al. 2020, *MNRAS*, 497, 917, doi: [10.1093/mnras/staa1920](https://doi.org/10.1093/mnras/staa1920)
- Madhusudhan, N., Rappaport, S., Podsiadlowski, P., & Nelson, L. 2008, *ApJ*, 688, 1235, doi: [10.1086/592237](https://doi.org/10.1086/592237)
- Makishima, K., Kubota, A., Mizuno, T., et al. 2000, *ApJ*, 535, 632, doi: [10.1086/308868](https://doi.org/10.1086/308868)
- Motch, C., Pakull, M. W., Soria, R., Grisé, F., & Pietrzyński, G. 2014, *Nature*, 514, 198, doi: [10.1038/nature13730](https://doi.org/10.1038/nature13730)
- Pakull, M. W., & Mirioni, L. 2002, arXiv e-prints, astro, doi: [10.48550/arXiv.astro-ph/0202488](https://doi.org/10.48550/arXiv.astro-ph/0202488)
- Pakull, M. W., & Mirioni, L. 2003, in *Revista Mexicana de Astronomia y Astrofisica Conference Series*, Vol. 15, *Revista Mexicana de Astronomia y Astrofisica Conference Series*, ed. J. Arthur & W. J. Henney, 197–199
- Patruno, A., & Zampieri, L. 2008, *MNRAS*, 386, 543, doi: [10.1111/j.1365-2966.2008.13063.x](https://doi.org/10.1111/j.1365-2966.2008.13063.x)
- Pinto, C., Middleton, M. J., & Fabian, A. C. 2016, *Nature*, 533, 64, doi: [10.1038/nature17417](https://doi.org/10.1038/nature17417)
- Pinto, C., Alston, W., Soria, R., et al. 2017, *MNRAS*, 468, 2865, doi: [10.1093/mnras/stx641](https://doi.org/10.1093/mnras/stx641)
- Pinto, C., Soria, R., Walton, D. J., et al. 2021, *MNRAS*, 505, 5058, doi: [10.1093/mnras/stab1648](https://doi.org/10.1093/mnras/stab1648)
- Quast, M., Langer, N., & Tauris, T. M. 2019, *A&A*, 628, A19, doi: [10.1051/0004-6361/201935453](https://doi.org/10.1051/0004-6361/201935453)
- Ramsey, C. J., Williams, R. M., Gruendl, R. A., et al. 2006, *ApJ*, 641, 241, doi: [10.1086/499070](https://doi.org/10.1086/499070)
- Read, A. M., & Pietsch, W. 2001, *A&A*, 373, 473, doi: [10.1051/0004-6361:20010636](https://doi.org/10.1051/0004-6361:20010636)
- Roberts, T. P., Gladstone, J. C., Goulding, A. D., et al. 2011, *Astronomische Nachrichten*, 332, 398, doi: [10.1002/asna.201011508](https://doi.org/10.1002/asna.201011508)
- Roberts, T. P., Goad, M. R., Ward, M. J., & Warwick, R. S. 2003, *MNRAS*, 342, 709, doi: [10.1046/j.1365-8711.2003.06593.x](https://doi.org/10.1046/j.1365-8711.2003.06593.x)
- Rodríguez Castillo, G. A., Israel, G. L., Belfiore, A., et al. 2020, *ApJ*, 895, 60, doi: [10.3847/1538-4357/ab8a44](https://doi.org/10.3847/1538-4357/ab8a44)
- Russell, D. M., Yang, Y. J., Gladstone, J. C., Wiersema, K., & Roberts, T. P. 2011, *Astronomische Nachrichten*, 332, 371, doi: [10.1002/asna.201011502](https://doi.org/10.1002/asna.201011502)
- Sathyaprakash, R., Roberts, T. P., Walton, D. J., et al. 2019, *MNRAS*, 488, L35, doi: [10.1093/mnras/slz086](https://doi.org/10.1093/mnras/slz086)
- Shao, Y., Li, X.-D., & Dai, Z.-G. 2019, *ApJ*, 886, 118, doi: [10.3847/1538-4357/ab4d50](https://doi.org/10.3847/1538-4357/ab4d50)
- Soria, R., & Kong, A. 2016, *MNRAS*, 456, 1837, doi: [10.1093/mnras/stv2671](https://doi.org/10.1093/mnras/stv2671)

- Soria, R., Pakull, M. W., Motch, C., et al. 2021, MNRAS, 501, 1644, doi: [10.1093/mnras/staa3784](https://doi.org/10.1093/mnras/staa3784)
- Tanaka, T., & Washimi, H. 2002, Science, 296, 321, doi: [10.1126/science.1069425](https://doi.org/10.1126/science.1069425)
- Tao, L., Feng, H., Kaaret, P., Grisé, F., & Jin, J. 2012, ApJ, 758, 85, doi: [10.1088/0004-637X/758/2/85](https://doi.org/10.1088/0004-637X/758/2/85)
- Tziamtzis, A., Lundqvist, P., Gröningsson, P., & Nasoudi-Shoar, S. 2011, A&A, 527, A35, doi: [10.1051/0004-6361/201015576](https://doi.org/10.1051/0004-6361/201015576)
- Urquhart, R., Soria, R., Johnston, H. M., et al. 2018, MNRAS, 475, 3561, doi: [10.1093/mnras/sty014](https://doi.org/10.1093/mnras/sty014)
- Vinokurov, A., Fabrika, S., & Atapin, K. 2013, Astrophysical Bulletin, 68, 139, doi: [10.1134/S1990341313020028](https://doi.org/10.1134/S1990341313020028)
- . 2018, ApJ, 854, 176, doi: [10.3847/1538-4357/aaa6c](https://doi.org/10.3847/1538-4357/aaa6c)
- Walton, D. J., Middleton, M. J., Pinto, C., et al. 2016, ApJL, 826, L26, doi: [10.3847/2041-8205/826/2/L26](https://doi.org/10.3847/2041-8205/826/2/L26)
- Wang, B., Chen, W.-C., Liu, D.-D., et al. 2021, MNRAS, 506, 4654, doi: [10.1093/mnras/stab2032](https://doi.org/10.1093/mnras/stab2032)
- Yao, Y., & Feng, H. 2019, ApJL, 884, L3, doi: [10.3847/2041-8213/ab44c7](https://doi.org/10.3847/2041-8213/ab44c7)
- Zhou, C., Bian, F., Feng, H., & Huang, J. 2022, ApJ, 935, 38, doi: [10.3847/1538-4357/ac815f](https://doi.org/10.3847/1538-4357/ac815f)